8-8-2016

Mitochondrial Akt Regulation of Hypoxic Tumor Reprogramming.

Young Chan Chae
The Wistar Institute

Valentina Vaira
Istituto Nazionale Genetica Molecolare; Fondazione IRCCS Ca' Granda Ospedale Maggiore Policlinico; University of Milan

M. Cecilia Caino
The Wistar Institute

Hsin-Yao Tang
University of Milan

Jae Ho Seo
The Wistar Institute

Recommended Citation

Authors

Young Chan Chae, Valentina Vaira, M. Cecilia Caino, Hsin-Yao Tang, Jae Ho Seo, Andrew V. Kossenkov, Luisa Ottobrini, Cristina Martelli, Giovanni Lucignani, Irene Bertolini, Marco Locatelli, Kelly G. Bryant, Jagadish C. Ghosh, Sofia Lisanti, Bonsu Ku, Silvano Bosari, Lucia R. Languino, David W. Speicher, and Dario C. Altieri

MITOCHONDRIAL Akt REGULATION OF HYPOXIC TUMOR REPROGRAMMING

Young Chan Chae[1], **Valentina Vaira**[2,3,4], **M. Cecilia Caino**[1], **Hsin-Yao Tang**[4], **Jae Ho Seo**[1], **Andrew V. Kossenkov**[5], **Luisa Ottobrini**[4,6], **Cristina Martelli**[4], **Giovanni Lucignani**[7,8], **Irene Bertolini**[3,4], **Marco Locatelli**[9], **Kelly G. Bryant**[1], **Jagadish C. Ghosh**[1], **Sofia Lisanti**[1], **Bonsu Ku**[10], **Silvano Bosari**[3,4], **Lucia R. Languino**[11], **David W. Speicher**[5,12], and **Dario C. Altieri**[1]

[1]Prostate Cancer Discovery and Development Program, Tumor Microenvironment and Metastasis Program, The Wistar Institute, Philadelphia, PA 19104, USA

[2]Istituto Nazionale Genetica Molecolare "Romeo and Enrica Invernizzi", Milan 20122, Italy

[3]Division of Pathology, Fondazione IRCCS Ca' Granda Ospedale Maggiore Policlinico, Milan 20122, Italy

[4]Department of Pathophysiology and Transplantation, University of Milan, Milan 20122, Italy

[5]Center for Systems and Computational Biology, The Wistar Institute, Philadelphia, PA 19104, USA

[6]Institute for Molecular Bioimaging and Physiology (IBFM), National Research Council (CNR), Milan 20090, Italy

[7]Department of Health Sciences, University of Milan, Milan 20142, Italy

[8]Department of Diagnostic Services, Unit of Nuclear Medicine, San Paolo Hospital, Milan 20142, Italy

[9]Division of Neurosurgery, Fondazione IRCCS Ca' Granda-Ospedale Maggiore Policlinico, Milan 20122, Italy

[10]Functional Genomics Research Center, Korea Research Institute of Bioscience and Biotechnology. 125 Gwahak-ro, Yuseong-gu, Daejeon 305-806, Republic of Korea

Correspondence to: Dario C. Altieri, M.D., The Wistar Institute, 3601 Spruce Street, Philadelphia, PA 19104, Tel. (215) 495-6970; (215) 495-2638; daltieri@wistar.org.

[11]Department of Cancer Biology, Kimmel Cancer Center, Thomas Jefferson University, Philadelphia, PA 19107, USA

[12]Molecular and Cellular Oncogenesis Program, The Wistar Institute, Philadelphia, PA 19104, USA

SUMMARY

Hypoxia is a universal driver of aggressive tumor behavior, but the underlying mechanisms are not completely understood. Using a phosphoproteomics screen, we now show that active Akt accumulates in the mitochondria during hypoxia and phosphorylates pyruvate dehydrogenase kinase 1 (PDK1) on Thr346 to inactivate the pyruvate dehydrogenase complex. In turn, this pathway switches tumor metabolism towards glycolysis, antagonizes apoptosis and autophagy, dampens oxidative stress, and maintains tumor cell proliferation in the face of severe hypoxia. Mitochondrial Akt-PDK1 signaling correlates with unfavorable prognostic markers and shorter survival in glioma patients and may provide an "actionable" therapeutic target in cancer.

Keywords

Mitochondria; Akt; PDK1; hypoxia; metabolism; tumor cell proliferation

INTRODUCTION

Hypoxia is a nearly universal feature of tumor growth (Hockel and Vaupel, 2001), conferring worse disease outcome via protection from apoptosis (Graeber et al., 1996), resistance to therapy (Tredan et al., 2007), and enhanced metastatic competence (Cox et al., 2015). This pathway requires the transcriptional activity of hypoxia-inducible factor 1 (HIF1), a master regulator of oxygen homeostasis (Keith et al., 2012) that becomes stabilized upon drops in oxygen pressure by escaping prolyl hydroxylation and proteasome-dependent destruction by the von Hippel-Lindau tumor suppressor (Semenza, 2013). In turn, nuclear localized HIF1 contributes to oncogene signaling (Mazumdar et al., 2010), angiogenesis (Ravi et al., 2000), cell invasion (Gilkes et al., 2014), and tumor metabolic reprogramming.

In this context, mitochondria are the primary site of hypoxia-induced metabolic reprogramming in tumors (Denko, 2008). This response involves HIF1-dependent transcription of mitochondrial pyruvate dehydrogenase kinase (PDK) (Kim et al., 2006; Papandreou et al., 2006), which in turn phosphorylates the pyruvate dehydrogenase complex (PDC) on three separate sites (Patel et al., 2014). By suppressing the oxidative decarboxylation of pyruvate into acetyl-CoA (Patel et al., 2014), an active PDK shuts off oxidative phosphorylation, lowers the production of toxic ROS, and switches tumor bioenergetics towards glycolysis (Denko, 2008), a driver of more aggressive disease traits (Gatenby and Gillies, 2004). What has remained unclear, however, is whether HIF1-dependent transcription is the sole mechanism for PDK activation in hypoxia (Kim et al., 2006; Papandreou et al., 2006), and the existence of other potential regulators of this response has not been widely investigated. In this study, we examined mechanisms of the tumor response to hypoxia.

RESULTS

A mitochondrial Akt phosphoproteome in hypoxia

We began this study by profiling the mitochondrial phosphoproteome of prostate adenocarcinoma PC3 cells exposed to severe hypoxia (<0.5% oxygen for 48 hr) versus normoxia. A total of 4,236 phosphosites were identified in the phosphopeptide-enriched samples, with a large number of changes in phosphorylation level in hypoxia/normoxia samples (Figures 1A and S1A). In total, 1,329 phosphosites showed a significant change (minimum fold-change of 1.6) in at least one sample analyzed (Figure 1A). By bioinformatics analysis, the mitochondrial phosphoproteome in hypoxia contained regulators of organelle integrity, bioenergetics, gene regulation and proteostasis (Figure 1B), which are functionally implicated in tumor cell proliferation, motility, invasion and apoptosis (Figure S1B). To complement these data, we also examined changes in the global mitochondrial proteome in hypoxia versus normoxia. A total of 5,583 proteins were identified in this analysis, and 267 of these proteins showed a significant change in hypoxia/normoxia samples (Figure S1C). Many of the phosphosites were not modulated at the protein level, suggesting that these phosphorylation events were independent of protein expression. In addition, the hypoxia-regulated mitochondrial phosphoproteome contained a discrete "Akt signature" (Figure 1A), characterized by increased phosphorylation of six Akt target proteins in hypoxia versus normoxia (Figure 1C).

Based on these results, we next looked at a role of Akt in the tumor response to hypoxia. Exposure of PC3 cells to hypoxia resulted in increased recruitment of Akt to mitochondria, whereas the cytosolic levels of Akt were unchanged between hypoxia and normoxia (Figures 1D and S1D). The hypoxia-regulated pool of mitochondrial Akt was "active" as it was phosphorylated on Ser473 (Figure 1D) and persisted for up to 24 hr after re-oxygenation (Figures 1E and S1E). Consistent with these results, hypoxia was accompanied by increased phosphorylation of a set of mitochondrial proteins recognized by an antibody to the Akt consensus phosphorylation sequence, RxRxxS/T (Akt cons Ab) (Figure 1F). Preincubation of mitochondrial extracts with Akt cons Ab (Figure 1F), or silencing Akt2 by small interfering RNA (siRNA) (Figure S1F), removed the mitochondrial proteins recognized by Akt cons Ab in hypoxia, confirming the specificity of this response and Akt-directed phosphorylation activity in mitochondria in hypoxia. Silencing Akt1 had minimal effect (Figure S1F). siRNA silencing of HIF1α did not affect Akt recruitment to mitochondria in hypoxia (Figure S1G), suggesting that this pathway did not require HIF1-dependent transcription. In addition, depletion of HIF1α did not affect Akt levels in the cytosol or mitochondria under normoxic conditions, whereas phosphorylated Akt2 levels were increased in the cytosol in response to hypoxia (Figure S1G). As detected by Akt cons Ab, the expression levels of downstream Akt-phosphorylated target molecules were unchanged in normoxic or hypoxic conditions (Figure 1F). In response to hypoxia, active Akt was found predominantly in the mitochondrial inner membrane, and, to a lesser extent, the matrix (Figure S1H).

The mechanism(s) of how Akt is recruited to mitochondria in hypoxia was further investigated. We found that blocking the chaperone activity of heat shock protein-90

(Hsp90) with 17-allylaminogeldanamycin (17-AAG) prevented the accumulation of mitochondrial Akt in hypoxia (Figure 1G). Also, scavenging mitochondrial ROS with MitoTempo (MT) inhibited Akt recruitment to mitochondria (Figure 1H). The antioxidant N-acetyl cysteine (NAC) had no effect (Figure 1H), identifying mitochondria-derived ROS as a critical stimulus for mitochondrial accumulation of Akt in hypoxia.

PDK1 is a phosphorylation target of mitochondrial Akt in hypoxia

We next set up a 1D proteomics screen to identify mitochondrial proteins phosphorylated by Akt in hypoxia (Figure 2A). Immune complexes precipitated with Akt cons Ab from normoxic or hypoxic PC3 cells contained bands with ~35 to ~120 kDa molecular weight that were more abundant in hypoxia (Figure S2A). Preclearing mitochondrial extracts with Akt cons Ab removed most of these proteins, validating the specificity of the immunoprecipitation step. From these experiments, we identified by mass spectrometry 84 high-confidence Akt substrates differentially expressed in hypoxia (Table S1). Sixteen of these molecules were known mitochondrial proteins (Figure 2B), including hypoxia- and HIF1-regulated effectors of bioenergetics (UGP2, SLC2A1, PDK1, HK2), extracellular matrix remodeling (P4HA1), Ca^{2+} homeostasis at the ER-mitochondria interface (Ero1L), oxidative phosphorylation (LonP1, IBA57), and metabolism (Acot9). Due to previously published work suggesting the importance of PDK1 in the tumor hypoxic response, we next focused on PDK1 as a potential substrate of mitochondrial Akt in hypoxia. In kinase assays, active Akt1 or Akt2 readily phosphorylated PDK1, as well as control GSK3β, as determined by Western blotting with Akt cons Ab (Figure 2C). This phosphorylation event was selective for PDK1, as related PDK2, PDK3 or PDK4 isoforms were unreactive (Figure 2D). In addition, PDK1 immune complexes reacted with Akt cons Ab preferentially in hypoxia (Figure 2E), and reciprocally, immune complexes precipitated with Akt cons Ab in hypoxia contained PDK1 (Figure S2B), consistent with the model of Akt phosphorylation of PDK1 in hypoxia.

We next looked for potential Akt phosphorylation sites in PDK1 by LC-MS/MS analysis of chymotrypsin digests of Akt-phosphorylated PDK1 in a kinase assay separated by SDS-PAGE (Figure S2C). We identified Thr346 (T346) in a number of PDK1 chymotryptic peptides, including the sequence STAPRPRVEpTSRAVPL (m/z=908.9751) as the sole phospho-amino acid modified by Akt1 or Akt2, compared to control (Figure 2F). The PDK1 sequence surrounding T346 matched an Akt consensus phosphorylation site, RxRxxS/T (Figure S2D), which was not present in PDK2, PDK3 or PDK4 (Figure S2E). Consistent with these data, active Akt2 phosphorylated wild type (WT) PDK1 but not a phosphorylation-defective Thr346→Ala (T346A) PDK1 mutant in transfected PC3 cells (Figure 2G). In the PDK1 crystal structure, T346 is predicted to localize to a flexible, "ATP lid" hinge region (Figure 2H), positioned to affect ATP loading and kinase activation.

To independently validate these findings, we next generated a phospho-specific antibody to phosphorylated T346 (pT346 Ab) in PDK1. The pT346 Ab dose-dependently reacted with the phosphorylated PDK1 peptide CAPRPRVE(pT)SRAVPLA, but not the non-phosphorylated sequence (Figure S2F). A second antibody raised against the non-phosphorylated sequence recognized the non-phosphorylated PDK1 peptide (Figure S2G).

Under these conditions, pT346 Ab reacted with Akt2-phosphorylated WT PDK1, but not T346A PDK1 mutant (Figure 2I). Consistent with the model that T346 phosphorylation is hypoxia-sensitive, WT PDK1, but not T346A PDK1, precipitated from hypoxic PC3 cells reacted with pT346 Ab (Figure 2J). pT346 Ab only weakly reacted with WT or T346A PDK1 precipitated from normoxic cells (Figure 2J).

Finally, we generated clones of PC3 cells stably silenced for endogenous PDK1 by short hairpin RNA (shRNA). pT346 Ab did not react with these cells in normoxia (Figure S2H). In contrast, pLKO transfectants reacted with pT346 Ab in hypoxia, and this response was abolished by shRNA silencing of PDK1 (Figure S2H).

Akt-PDK1 phosphorylation axis in hypoxia

Expression of WT PDK1 in hypoxic PC3 cells increased the phosphorylation of the E1α catalytic subunit (PDHE1) of the PDC (Figure 3A) on site 1 (Ser264 in the mature protein), one of three regulatory phosphorylation sites (Patel et al., 2014). Conversely, expression of T346A PDK1 mutant reduced PDHE1 phosphorylation in hypoxia (Figure 3A), and no PDHE1 phosphorylation was detected in normoxia (Figure 3A). Immune complexes of WT or T346A PDK1 mutant contained comparable amounts of the PDC component, PDHE1α, suggesting that T346 does not contribute to a PDK1-PDC complex (Figure S3A). In a kinase assay, active Akt2 increased PDK1 phosphorylation of PDHE1 (Figure 3B). While WT PDK1 phosphorylated PDHE1 in the presence of Akt2 (Figure 3C), T346A PDK1 mutant was ineffective (Figure 3C). Consistent with these data, increased PDHE1 phosphorylation was detected only in the presence of Akt2 and PDK1, but not PDK2, PDK3 or PDK4 (Figure S3B). Silencing of Akt2 inhibited PDHE1 phosphorylation in hypoxia, whereas Akt1 knockdown only had a partial effect (Figure 3D). As a complementary approach, we used a pan-Akt small molecule inhibitor, MK2206, which indistinguishably suppressed Akt phosphorylation in hypoxia and normoxia (Figure S3C). Incubation of PC3 cells with MK2206 suppressed PDHE1 phosphorylation in hypoxia (Figure 3E). This response was specific because PDK1 immunoprecipitated from MK2206-treated cells also failed to phosphorylate PDHE1 in a kinase assay in hypoxia (Figure S3D). In normoxia, MK2206 had no effect on PDHE1 phosphorylation in cell extracts (Figure 3E) or in a kinase assay with immunoprecipitated PDK1 (Figure S3D), validating the specificity of Akt-directed phosphorylation in hypoxic conditions.

As an independent approach, we next generated WT or kinase-dead (KD) Akt2 constructs targeted to the mitochondria by the cytochrome c oxidase subunit 8 mitochondrial import sequence. Similar to the endogenous protein, mitochondrial-targeted Akt2 accumulated in the various submitochondrial fractions (Figure S3E). Functionally, mitochondrial-targeted Akt2-KD inhibited PDHE1 phosphorylation in hypoxic PC3 cells (Figure 3F), whereas non-mitochondrial targeted Akt2-KD had no effect. There was no PDHE1 phosphorylation in the cytosol of hypoxic or normoxic tumor cells, and Akt2-KD or mitochondrial-targeted Akt2-KD had no effect in these settings (Figure S3F). Reciprocally, forced expression of mitochondrial-targeted WT Akt2 was sufficient to increase PDHE1 phosphorylation even in the absence of hypoxia (Figure S3G).

Finally, we reconstituted PDK1-depleted cells with various PDK1 cDNAs. Expression of WT PDK1 in these settings restored PDHE1 phosphorylation in hypoxia, whereas T346A PDK1 mutant had no effect (Figure 3G). With respect to its enzymatic function, PDK1 knockdown increased PDH activity in normoxic PC3 cells (Figure 3H). Hypoxic cells showed reduced PDH activity, and this response was partially rescued by shRNA silencing of PDK1 (Figure 3H). Reconstitution of these cells with WT PDK1, but not T346A PDK1 mutant, suppressed PDH activity in hypoxia (Figure 3I). In addition, expression of Akt-KD or mitochondrial-targeted Akt-KD in PC3 cells had no effect on PDH activity in normoxia, but modestly elevated PDH function in hypoxia (Figure S3H), consistent with loss of an Akt-regulated inhibitory function of PDK1 in these settings. Vector or non-mitochondrial targeted Akt2-KD had no effect (Figure S3H).

Mitochondrial Akt-PDK1 phosphorylation controls tumor metabolic reprogramming

To understand how mitochondrial Akt-PDK1 signaling affects tumor behavior, we first looked at potential changes in cancer metabolism. Consistent with previous studies, hypoxia stimulated glycolytic metabolism in tumor cells, characterized by increased glucose consumption (Figure 3J) and lactate production (Figure 3K). Mitochondrial Akt-PDK1 signaling was important for this response, as PDK1 knockdown reduced glucose consumption in hypoxia, whereas reconstitution of targeted cells with WT PDK1, but not T346A PDK1 mutant, restored glycolysis (Figure 3J). Similarly, Akt inhibition with MK2206 (Figure 3K) or silencing of Akt2 (Figure 3L) impaired metabolic reprogramming, reducing lactate production in hypoxia. Normoxic cultures were not affected (Figures 3K and 3L), and Akt1 knockdown had only partial effect (Figure 3L). Consistent with a metabolic switch towards glycolysis (Kim et al., 2006; Papandreou et al., 2006), PC3 cells reconstituted with WT PDK1 exhibited reduced oxygen consumption, a marker of oxidative phosphorylation, whereas expression of T346A PDK1 mutant restored oxygen consumption (Figure 3M), further supporting a role of mitochondrial Akt-PDK1 signaling in hypoxic metabolic reprogramming.

Mitochondrial Akt-PDK1 phosphorylation in vivo

When analyzed in time-course experiments, hypoxia increased phosphorylation of Akt1 and Akt2, as well as PDHE1 starting at 3 and 6 hr, respectively (Figure S4A). The overall hypoxic response under these conditions was cell type-specific. Akt inhibition strongly reduced PDHE1 phosphorylation in prostate adenocarcinoma (DU145), lung adenocarcinoma (A549) and glioblastoma (LN229), but had no effect on PDHE1 phosphorylation in breast adenocarcinoma cells MCF-7 (ER$^+$) or MDA-231 (ER$^-$) (Figure S4B). Knockdown of PTEN in MCF-7 cells increased PDHE1 phosphorylation in normoxia and, to a lesser extent, hypoxia, whereas LN229 cells were unaffected (Figure S4C), suggesting that PTEN status may differentially affect hypoxia-stimulated mitochondrial Akt-PDK1 signaling depending on the tumor cell type.

To examine a more "physiologic" model of tumor hypoxia, we next looked at 3D cultures of patient-derived, stem cell-enriched GBM neurospheres (Di Cristofori et al., 2015). These cultures become hypoxic in their "core", as determined by expression of a hypoxia probe (Figures 4A and S4D and S4E). Under these conditions, GBM neurospheres exhibited

strong phosphorylation of PDK1, as determined by immunofluorescence with pT346 Ab (Figure 4A). Conversely, differentiated GBM cells depleted of stem cells and growing as monolayers were normoxic, contained cytosolic HIF1α, and did not react with pT346 Ab (Figure 4A). Pre13 absorption of pT346 Ab with the immunizing peptide abolished reactivity with GBM (Figure S4D).

Next, we looked at Akt phosphorylation of PDK1 in primary, patient-derived GBM tissue samples (Table S2). GBMs with a high score (2) for nuclear HIF1α showed increased phosphorylation of PDK1 by Akt (pT346 Ab), as well as phosphorylation of PDHE1 and Src, a major determinant of glioma invasiveness (Du et al., 2009), in hypoxic areas (Figures 4B and S4F). In contrast, GBMs with undetectable nuclear HIF1α (score = 0) showed low to undetectable levels of PDK1-PDHE1 phosphorylation (Figures 4C and S4F). In these patients, phosphorylation of PDK1 (pT346 Ab) (Figure 4D) or PDHE1 phosphorylation (Figure 4E) correlated with expression of nuclear HIF1α. Reciprocally, PDHE1 phosphorylation correlated with the expression of Akt-phosphorylated PDK1 (pT346 Ab) (Figure 4F), reinforcing a link between hypoxia and mitochondrial Akt-PDK1 phosphorylation in primary patient samples.

Mitochondrial Akt-PDK1 regulation of tumor cell proliferation in hypoxia

To test a role of a mitochondrial Akt-PDK1 signaling in tumor growth in vivo, we first utilized human U251 GBM cells expressing a luciferase reporter under the control of a HIF1-responsive element (HRE) and a mCherry reporter under a constitutive PGK promoter to quantify cell viability. Stereotactic intracranial injection of these cells in immunocompromised mice gave rise to GBMs characterized by HIF1-directed luciferase activity and reactivity with a hypoxia-sensitive marker (Figures 5A and 5B). Despite low oxygenation, these orthotopic GBMs remained viable, as determined by high mCherry expression (Figures 5A and 5B) and exhibited a time-dependent increase in the number of mitotic tumor cells (Figure S5A). These proliferating cells stained intensely positive for Akt-phosphorylated PDK1 (Figures 5C and S5B and S5C), correlating with increased HIF1 activity (Figure S5D). PDHE1 was also highly phosphorylated in intracranial GBMs (Figure 5C).

We next tested the requirement of mitochondrial Akt-PDK1 signaling in regulating proliferation under hypoxic conditions. siRNA knockdown of Akt1 or Akt2 (Figure 5D) or stable shRNA knockdown of PDK1 (Figure 5E) suppressed tumor cell proliferation in hypoxia. Normoxic cultures were partially affected (Figures 5D and 5E). When cells were analyzed for cell cycle transitions, MK2206 or the PDK1 inhibitor dichloroacetate (DCA) suppressed S-phase progression in hypoxia and increased the population of tumor cells in G1/sub-G1 phase (Figure S5E). Finally, stable silencing of PDK1 abolished PC3 colony formation in hypoxia, a marker of tumorigenicity (Figures 5F and 5G), whereas normoxic growth was not significantly affected. Together, these data point to an important role of mitochondrial Akt-PDK1 signaling in maintaining tumor cell proliferation in hypoxia.

Mitochondrial Akt regulation of stress signaling in hypoxia

The downstream implications of defective mitochondrial Akt-PDK1 signaling were next investigated. First, inhibition of Akt with MK2206 (Figure 6A) or stable shRNA silencing of PDK1 (Figure 6B) increased aberrant ROS production in tumor cells, especially in hypoxia. This was associated with decreased tumor cell viability (Figure 6C), and appearance of cleaved caspase 3 (Figure 6D), a marker of apoptosis. In normoxia, cleaved caspase 3 was undetectable. Confirming the specificity of this response, exposure of tumor cells to a small molecule inhibitor of PI3K, PX-866 did not result in caspase activation (Figure 6D). Reconstitution of these cells with WT PDK1, but not T346A PDK1 mutant, partially rescued tumor cell viability in hypoxia (Figure 6E). Normoxic cultures were not affected, further supporting a role of PDK1 signaling selectively in hypoxia.

As a second downstream pathway of tumor maintenance modulated by bioenergetics, we next observed that stable knockdown of PDK1 (Figure 6F) or siRNA silencing of Akt1 or Akt2 (Figure 6G) in hypoxia increased the phosphorylation of the energy stress sensor, AMP-regulated kinase (AMPK). This response was associated with concomitant activation of autophagy, as determined by LC3 conversion to a lipidated form (Figures 6F and 6G), and punctate LC3 fluorescence staining (Figures 6H and 6I). Normoxic cultures showed a minimal level of autophagy induction after PDK1 silencing (Figures 6F and 6G and S6A). In PDK1-depleted cells, re-expression of WT PDK1, but not T346A PDK1 mutant, attenuated AMPK phosphorylation and reduced autophagy in hypoxia (Figures 6H and 6I and S6B).

Requirement of hypoxic mitochondrial reprogramming for tumor growth in vivo

Next, we asked if mitochondrial Akt-PDK1 signaling was important for tumor growth in vivo. shRNA silencing of PDK1 significantly impaired the growth of PC3 xenograft tumors implanted in immunocompromised mice (Figure 7A). Re-expression of WT PDK1 in these cells restored tumor growth in vivo (Figures 7B and 7C), whereas T346A PDK1 mutant further impaired tumor growth (Figure 7C). By immunohistochemistry, PC3 tumors harboring WT PDK1 showed increased cell proliferation, reduced apoptosis and lower levels of autophagy, compared to tumors reconstituted with T346A PDK1 mutant (Figures 7D and 7E). In addition, tumors with loss of endogenous PDK1 showed a trend towards increased apoptosis and heightened autophagy in vivo, whereas tumor cell proliferation by Ki-67 staining was unchanged (Figures 7F and G). Taken together, these results suggest that mitochondrial Akt-PDK1 signaling promotes tumor adaptation to hypoxia, and specifically enables continued tumor cell proliferation despite an unfavorable microenvironment (Figure 7H).

To test the relevance of this model in human cancer, we next looked at the prognostic impact of Akt phosphorylation of PDK1 in a clinically-annotated cohort of 116 glioma patients (Table S3). Undetectable in normal brain parenchyma, the expression of Akt phosphorylated PDK1 on T346 progressively increased in gliomas, with the highest reactivity observed in glioblastoma (Figures 8A and 8B). PDK1 phosphorylation on T346 segregated with other markers of disease progression, including HIF1α expression (Figure 8C), wild type status of isocitrate dehydrogenase-1 (*IDH1*) (Figure 8D), and unmethylated MGMT promoter (Figure 8E). Consistent with this prognostic profile, elevated expression of Akt-phosphorylated

PDK1, as determined by ROC curves analysis (Figures S7A and S7B), was significantly associated with reduced overall survival in patients with gliomas (p=0.006; HR=2.2; 95%CI: 1.17–4.12; Figure 8F) as well as patients with GBM (p=0.032; HR=2.03; 95%CI: 0.95–4.32; Figure 8G).

DISCUSSION

In this study, we have shown that hypoxia, a universal driver of malignancy, promotes the recruitment of active Akt to mitochondria of tumor cells. In turn, mitochondrial Akt, in particular Akt2, phosphorylates the bioenergetics regulator PDK1 on a Thr346 target site, resulting in increased kinase activity and phosphorylation of its downstream substrate in the PDC, PDHE1α. This pathway improves tumor fitness, stimulating glycolysis, countering autophagy and apoptosis, dampening oxidative stress, and enabling continued cell proliferation in face of severe hypoxia in vivo. Accordingly, mitochondrial Akt-PDK1 signaling emerged as a powerful negative prognostic factor in glioma patients, correlating with markers of unfavorable outcome and shortened survival.

Akt is an essential signaling node exploited in most cancers, integrating growth factor responses with mechanisms of cell proliferation, survival and bioenergetics (Manning and Cantley, 2007). The role of this pathway as a regulator of tumor adaptation to hypoxia has not been previously described, and its spatial arrangement in subcellular compartments, in particular mitochondria, has only recently begun to emerge (Ghosh et al., 2015). Data presented here suggest that the recruitment of predominantly active Akt to mitochondria during hypoxia (Santi and Lee, 2010) may be part of a broader stress response in tumors, enabled by the chaperone function of cytosolic Hsp90 in mitochondrial pre-protein import (Young et al., 2003) and mitochondrial ROS production, which may participate in subcellular trafficking of signaling molecules (Nakahira et al., 2006), including mitochondrial import (Fischer and Riemer, 2013).

In our phosphoproteomics screen, Akt recruitment to mitochondria was associated with a discrete Akt phosphorylation signature that included regulators of organelle homeostasis and glycolytic reprogramming in hypoxia, such as 6-phosphofructose-2-kinase/fructose-2,6-bisphosphatase 3 (PFKB3) and PDK1 (De Bock et al., 2013). In the case of PDK1, Akt phosphorylation took place exclusively in hypoxia, did not involve other PDK isoforms, and targeted a unique Thr346 site in the "ATP lid" (Zhang et al., 2015), ideally positioned to affect ATP loading, and kinase activation (Patel et al., 2014). Thr346 did not affect PDK1 binding to the PDC, thus differently from another proposed post-translational modification of PDK1 involving Tyr phosphorylation of the "ATP lid" (Hitosugi et al., 2011).

Extensively studied as part of HIF1 signaling (Semenza, 2013), the tumor response to hypoxia has been linked to metabolic reprogramming (Kim et al., 2006; Papandreou et al., 2006), with suppression of mitochondrial respiration in favor of glycolysis (Denko, 2008). However, there is evidence that this pathway may extend well beyond bioenergetics, as PDK1 signaling has been implicated in senescence (Kaplon et al., 2013), metastatic tropism (Dupuy et al., 2015), and multiple mechanisms of tumor maintenance (McFate et al., 2008). The fact that this response is "druggable" and that small molecule PDK1 inhibitors have

entered clinical testing in cancer patients (Michelakis et al., 2010) adds to the relevance of PDK1 signaling as a potential driver of tumor progression.

Against this backdrop, the pathway of mitochondrial Akt-PDK1 signaling described here appears ideally poised to affect a plethora of downstream signaling mechanisms important for tumor adaptation and improved fitness. This involves suppression of apoptosis via mitochondrial Akt phosphorylation of hexokinase-II at the outer membrane (Roberts et al., 2013) and cyclophilin D in the permeability transition pore (Ghosh et al., 2015), as well as inhibition of oxidative phosphorylation through Akt phosphorylation of PDK1 and subsequent inhibition of the PDC (Patel et al., 2014). In turn, this lowers the production of toxic ROS, prevents the phosphorylation of stress energy sensor, AMPK (Liang and Mills, 2013), and inhibits downstream activation of autophagy (White, 2012). Although these pathways have been implicated in both tumor suppression and oncogenesis (Liang and Mills, 2013; White, 2012), there is evidence that AMPK inhibition and suppression of autophagy may promote malignant expansion (White, 2012), and heightened metastatic competence (Caino et al., 2013), including in hypoxia (Liu et al., 2015), further compounding the more aggressive traits of glycolytic tumors (Gatenby and Gillies, 2004).

Here, a pivotal feature of mitochondrial Akt-PDK1 signaling was its activation in mitotic cells and requirement to support tumor cell proliferation in the face of hypoxia, in vivo. Whether this response can be entirely attributed to the suppression of ROS or involves other mechanisms of mitochondria-to-nuclei retrograde signaling (Jazwinski, 2013) remains to be elucidated. On the other hand, hypoxic reprogramming may participate in cell cycle transitions via regulation of p27 expression (Gardner et al., 2001) or Myc transcriptional activity (Gordan et al., 2007), and effector(s) of glycolysis have been linked to chromosomal segregation and mitotic progression, selectively in hypoxia (Jiang et al., 2014). In line with the broad impact of mitochondrial Akt-PDK1 signaling on multiple mechanisms of tumor adaptation, this pathway was found to have significant implications for disease progression in humans. Accordingly, expression of PDK1 phosphorylated on T346 was undetectable in normal brain, but increased steadily in the hypoxic environment of gliomas, including glioblastomas, segregated with unfavorable prognostic markers, and correlated with shortened overall survival in these patients. Although these results await further confirmation in larger patient cohorts, detection of Akt-phosphorylated PDK1 may provide an easily accessible biomarker for clinical decision-making in patients with gliomas, including glioblastoma (Wick et al., 2014).

Despite expectations for personalized, or precision medicine, small molecule antagonists of Akt and its associated signaling nodes, PI3K and mTOR (Manning and Cantley, 2007), have produced only limited responses in the clinic, hampered by drug resistance and significant toxicity (Fruman and Rommel, 2014). While these results may reflect mechanisms of tumor adaptation (Ghosh et al., 2015), including mitochondrial reprogramming (Caino et al., 2015), the identification of mitochondrial Akt (Ghosh et al., 2015) as a post-translational regulator of PDK1 activity and tumor progression may rationally repurpose Akt-directed molecular therapies as an approach to impair tumor adaptation to hypoxia. In this context, targeted inhibition of the mitochondrial pool of Akt may selectively disable a host of metabolic, survival and proliferative requirements for tumor fitness (McFate et al., 2008) and

reawaken endogenous tumor suppressor mechanisms important for anticancer activity in patients.

EXPERIMENTAL PROCEDURES

Patients

All patient-related studies were reviewed and approved by an Institutional Review Board at Fondazione IRCCS, Ca' Granda Ospedale Maggiore Policlinico Milan, Italy. A first cohort of 26 patients diagnosed with de novo glioma were enrolled at Fondazione IRCCS Ca' Granda Ospedale Maggiore Policlinico (Milan, Italy) between 2010 and 2011, and described previously (Di Cristofori et al., 2015). All patients were treated with surgical resection with curative intent. Gliomas were staged according to the WHO classification (Louis et al., 2007), and the clinicopathological and molecular characteristics of the patients' series used in this study are described in Table S2. This cohort was used to evaluate the expression of phosphoT346-PDK1 (pPDK1), phosphoPDHE1α (pPDHE1), phosphoT416-Src (pSrc) and nuclear HIF1α reactivity, by immunohistochemistry. Tissue microarrays (TMAs) of glioma or normal brain tissues were as described (Di Cristofori et al., 2015). Immunohistochemistry slides were digitalized using an Aperio scanner at 20× magnification, and HIF1α nuclear staining was quantified using a nuclear-specific algorithm implemented in Genie Histology Pattern Recognition software (Aperio, Leica Microsystems). To specifically quantify nuclear HIF1α expression in primary GBM culture, the Volocity algorithm that counts and displays red signals (HIF1α) within the Hoechst signal (nuclei) in each z-stack was used. A second series of 116 patients with *de novo* glioma who underwent surgery with curative intent between 2008 and 2009 and for which complete clinical and follow-up records were available (Table S3), was retrieved from the archives of the Pathology Division. This cohort was used in the present study to correlate the expression of Akt-phosphorylated PDK1 on T346 with prognostic markers of glioma progression, including nuclear HIF1α, MGMT promoter methylation and *IDH1* mutational status (wild type (WT)/R132H), and patients' overall survival.

Xenograft tumor growth studies

All experiments involving animals were approved by an Institutional Animal Care and Use Committee (IACUC) at The Wistar Institute in accordance with the Guide for the Care and Use of Laboratory Animals of the National Institutes of Health (NIH), or, alternatively, at the University of Milan, in compliance with the Italian Ministry of Health. In a first set of experiments, PC3 cells stably transduced with control pLKO or PDK1-directed shRNA were reconstituted with vector, WT PDK1 or T346A PDK1 mutant cDNA at 80% confluency, suspended in PBS, pH 7.4, and injected (0.2 ml containing 2×10^6 cells) s.c. into the flank of 6–8 week old male NOD SCID γ (NSG, NOD.Cg-*Prkdc^{scid} Il2rg^{tm1Wjl}*/SzJ) immunocompromised mice (Jackson Laboratory, 3 mice per condition/2 tumors per mouse). The width and length of superficial tumors were measured with a caliper at the indicated time intervals, and tumor volume was calculated according to the formula Vol= width^2 × length/2. After 21 days Xenograft tumors were harvested, fixed and processed for immunohistochemistry.

An orthotopic murine model of glioblastoma (GBM) was obtained by stereotactic injection (coordinates: 1.5 mm lateral to the bregma, 0 mm behind and 3.0 mm ventral to the dura) (Maes et al., 2009) of 1×10^5 U251-HRE-mCherry GBM cells in 2 μl of PBS into 7–8-week-old female nude mice (Harlan Laboratories) at day 0 (Lo Dico et al., 2014). Following surgery, mice were monitored for recovery until complete awakening. Six animals per time point were used and mice were euthanized after 20 or 34 days. Intracranial GBM samples were harvested from the various groups and processed for differential expression of phosphorylated PDK1 or PDHE1, HIF1α or Ki-67 by immunohistochemistry on serial sections.

Statistical analysis

Data were analyzed using the two-sided unpaired t or chi-square tests using a GraphPad software package (Prism 6.0) for Windows. Correlation parameters between immunohistochemical (IHC) scores in glioma patients and clinicopathological variables were derived using Mann-Whitney U test or chi-square test for continuous or discrete variable, respectively, using GraphPad Prism or MedCalc (Mariakerke, Belgium) statistical package. Receiver operating characteristics (ROC) curves method was used to test the accuracy of T346 phosphorylated PDK1 to correctly discriminate between glioma patients according to their survival status (alive or dead for the disease) and to generate cut-offs for phosphorylated PDK1 IHC score using the non-arbitrary criterion derived from the Youden's statistic (J, MedCalc Software) as described (Di Cristofori et al., 2015). The pPDK1 IHC score value that more accurately discriminated between alive or dead patients was >25 and >40 for gliomas or GBM patients, respectively (Youden criterion). Glioma patients were then sorted into low or highexpressor categories and Kaplan-Meier survival curves were compared using the Log-Rank test (MedCalc Software). Data are expressed as mean±SD or mean±SEM of replicates from a representative experiment out of at least two or three independent determinations. A p value of <0.05 was considered as statistically significant.

Supplementary Material

Refer to Web version on PubMed Central for supplementary material.

Acknowledgments

REFERENCES

Caino MC, Chae YC, Vaira V, Ferrero S, Nosotti M, Martin NM, Weeraratna A, O'Connell M, Jernigan D, Fatatis A, et al. Metabolic stress regulates cytoskeletal dynamics and metastasis of cancer cells. J Clin Invest. 2013; 123:2907–2920. [PubMed: 23921130]

Caino MC, Ghosh JC, Chae YC, Vaira V, Rivadeneira DB, Faversani A, Rampini P, Kossenkov AV, Aird KM, Zhang R, et al. PI3K therapy reprograms mitochondrial trafficking to fuel tumor cell invasion. Proc Natl Acad Sci U S A. 2015; 112:8638–8643. [PubMed: 26124089]

Cox TR, Rumney RM, Schoof EM, Perryman L, Hoye AM, Agrawal A, Bird D, Latif NA, Forrest H, Evans HR, et al. The hypoxic cancer secretome induces pre-metastatic bone lesions through lysyl oxidase. Nature. 2015; 522:106–110. [PubMed: 26017313]

De Bock K, Georgiadou M, Schoors S, Kuchnio A, Wong BW, Cantelmo AR, Quaegebeur A, Ghesquiere B, Cauwenberghs S, Eelen G, et al. Role of PFKFB3-driven glycolysis in vessel sprouting. Cell. 2013; 154:651–663. [PubMed: 23911327]

Denko NC. Hypoxia, HIF1 and glucose metabolism in the solid tumour. Nat Rev Cancer. 2008; 8:705–713. [PubMed: 19143055]

Di Cristofori A, Ferrero S, Bertolini I, Gaudioso G, Russo MV, Berno V, Vanini M, Locatelli M, Zavanone M, Rampini P, et al. The vacuolar H+ ATPase is a novel therapeutic target for glioblastoma. Oncotarget. 2015; 6:17514–17531. [PubMed: 26020805]

Du J, Bernasconi P, Clauser KR, Mani DR, Finn SP, Beroukhim R, Burns M, Julian B, Peng XP, Hieronymus H, et al. Bead-based profiling of tyrosine kinase phosphorylation identifies SRC as a potential target for glioblastoma therapy. Nat Biotechnol. 2009; 27:77–83. [PubMed: 19098899]

Dupuy F, Tabaries S, Andrzejewski S, Dong Z, Blagih J, Annis MG, Omeroglu A, Gao D, Leung S, Amir E, et al. PDK1-Dependent Metabolic Reprogramming Dictates Metastatic Potential in Breast Cancer. Cell Metab. 2015; 22:577–589. [PubMed: 26365179]

Fischer M, Riemer J. The mitochondrial disulfide relay system: roles in oxidative protein folding and beyond. Int J Cell Biol. 2013; 2013:742923. [PubMed: 24348563]

Fruman DA, Rommel C. PI3K and cancer: lessons, challenges and opportunities. Nat Rev Drug Discov. 2014; 13:140–156. [PubMed: 24481312]

Gardner LB, Li Q, Park MS, Flanagan WM, Semenza GL, Dang CV. Hypoxia inhibits G1/S transition through regulation of p27 expression. J Biol Chem. 2001; 276:7919–7926. [PubMed: 11112789]

Gatenby RA, Gillies RJ. Why do cancers have high aerobic glycolysis? Nat Rev Cancer. 2004; 4:891–899. [PubMed: 15516961]

Ghosh JC, Siegelin MD, Vaira V, Faversani A, Tavecchio M, Chae YC, Lisanti S, Rampini P, Giroda M, Caino MC, et al. Adaptive mitochondrial reprogramming and resistance to PI3K therapy. J Natl Cancer Inst. 2015; 107

Gilkes DM, Semenza GL, Wirtz D. Hypoxia and the extracellular matrix: drivers of tumour metastasis. Nat Rev Cancer. 2014; 14:430–439. [PubMed: 24827502]

Gordan JD, Bertout JA, Hu CJ, Diehl JA, Simon MC. HIF-2alpha promotes hypoxic cell proliferation by enhancing c-myc transcriptional activity. Cancer Cell. 2007; 11:335–347. [PubMed: 17418410]

Graeber TG, Osmanian C, Jacks T, Housman DE, Koch CJ, Lowe SW, Giaccia AJ. Hypoxia-mediated selection of cells with diminished apoptotic potential in solid tumours. Nature. 1996; 379:88–91. [PubMed: 8538748]

Hitosugi T, Fan J, Chung TW, Lythgoe K, Wang X, Xie J, Ge Q, Gu TL, Polakiewicz RD, Roesel JL, et al. Tyrosine phosphorylation of mitochondrial pyruvate dehydrogenase kinase 1 is important for cancer metabolism. Mol Cell. 2011; 44:864–877. [PubMed: 22195962]

Hockel M, Vaupel P. Tumor hypoxia: definitions and current clinical, biologic, and molecular aspects. J Natl Cancer Inst. 2001; 93:266–276. [PubMed: 11181773]

Jazwinski SM. The retrograde response: When mitochondrial quality control is not enough. Biochim Biophys Acta. 2013; 1833:400–409. [PubMed: 22374136]

Jiang Y, Li X, Yang W, Hawke DH, Zheng Y, Xia Y, Aldape K, Wei C, Guo F, Chen Y, et al. PKM2 regulates chromosome segregation and mitosis progression of tumor cells. Mol Cell. 2014; 53:75–87. [PubMed: 24316223]

Kaplon J, Zheng L, Meissl K, Chaneton B, Selivanov VA, Mackay G, van der Burg SH, Verdegaal EM, Cascante M, Shlomi T, et al. A key role for mitochondrial gatekeeper pyruvate dehydrogenase in oncogene-induced senescence. Nature. 2013; 498:109–112. [PubMed: 23685455]

Keith B, Johnson RS, Simon MC. HIF1alpha and HIF2alpha: sibling rivalry in hypoxic tumour growth and progression. Nat Rev Cancer. 2012; 12:9–22.

Kim JW, Tchernyshyov I, Semenza GL, Dang CV. HIF-1-mediated expression of pyruvate dehydrogenase kinase: a metabolic switch required for cellular adaptation to hypoxia. Cell Metab. 2006; 3:177–185. [PubMed: 16517405]

Liang J, Mills GB. AMPK: a contextual oncogene or tumor suppressor? Cancer Res. 2013; 73:2929–2935. [PubMed: 23644529]

Liu XD, Yao J, Tripathi DN, Ding Z, Xu Y, Sun M, Zhang J, Bai S, German P, Hoang A, et al. Autophagy mediates HIF2alpha degradation and suppresses renal tumorigenesis. Oncogene. 2015; 34:2450–2460. [PubMed: 24998849]

Lo Dico A, Valtorta S, Martelli C, Belloli S, Gianelli U, Tosi D, Bosari S, Degrassi A, Russo M, Raccagni I, et al. Validation of an engineered cell model for in vitro and in vivo HIF-1alpha evaluation by different imaging modalities. Mol Imaging Biol. 2014; 16:210–223. [PubMed: 24002614]

Louis DN, Ohgaki H, Wiestler OD, Cavenee WK, Burger PC, Jouvet A, Scheithauer BW, Kleihues P. The 2007 WHO classification of tumours of the central nervous system. Acta Neuropathol. 2007; 114:97–109. [PubMed: 17618441]

Maes W, Deroose C, Reumers V, Krylyshkina O, Gijsbers R, Baekelandt V, Ceuppens J, Debyser Z, Van Gool SW. In vivo bioluminescence imaging in an experimental mouse model for dendritic cell based immunotherapy against malignant glioma. J Neurooncol. 2009; 91:127–139. [PubMed: 18787761]

Manning BD, Cantley LC. AKT/PKB signaling: navigating downstream. Cell. 2007; 129:1261–1274. [PubMed: 17604717]

Mazumdar J, O'Brien WT, Johnson RS, LaManna JC, Chavez JC, Klein PS, Simon MC. O2 regulates stem cells through Wnt/beta-catenin signalling. Nat Cell Biol. 2010; 12:1007–1013. [PubMed: 20852629]

McFate T, Mohyeldin A, Lu H, Thakar J, Henriques J, Halim ND, Wu H, Schell MJ, Tsang TM, Teahan O, et al. Pyruvate dehydrogenase complex activity controls metabolic and malignant phenotype in cancer cells. J Biol Chem. 2008; 283:22700–22708. [PubMed: 18541534]

Michelakis ED, Sutendra G, Dromparis P, Webster L, Haromy A, Niven E, Maguire C, Gammer TL, Mackey JR, Fulton D, et al. Metabolic modulation of glioblastoma with dichloroacetate. Sci Transl Med. 2010; 2:31ra34.

Nakahira K, Kim HP, Geng XH, Nakao A, Wang X, Murase N, Drain PF, Wang X, Sasidhar M, Nabel EG, et al. Carbon monoxide differentially inhibits TLR signaling pathways by regulating ROS-induced trafficking of TLRs to lipid rafts. J Exp Med. 2006; 203:2377–2389. [PubMed: 17000866]

Papandreou I, Cairns RA, Fontana L, Lim AL, Denko NC. HIF-1 mediates adaptation to hypoxia by actively downregulating mitochondrial oxygen consumption. Cell Metab. 2006; 3:187–197. [PubMed: 16517406]

Patel MS, Nemeria NS, Furey W, Jordan F. The pyruvate dehydrogenase complexes: structure-based function and regulation. J Biol Chem. 2014; 289:16615–16623. [PubMed: 24798336]

Ravi R, Mookerjee B, Bhujwalla ZM, Sutter CH, Artemov D, Zeng Q, Dillehay LE, Madan A, Semenza GL, Bedi A. Regulation of tumor angiogenesis by p53- induced degradation of hypoxia-inducible factor 1alpha. Genes Dev. 2000; 14:34–44. [PubMed: 10640274]

Roberts DJ, Tan-Sah VP, Smith JM, Miyamoto S. Akt phosphorylates HK-II at Thr-473 and increases mitochondrial HK-II association to protect cardiomyocytes. J Biol Chem. 2013; 288:23798–23806. [PubMed: 23836898]

Santi SA, Lee H. The Akt isoforms are present at distinct subcellular locations. Am J Physiol Cell Physiol. 2010; 298:C580–C591. [PubMed: 20018949]

Semenza GL. HIF-1 mediates metabolic responses to intratumoral hypoxia and oncogenic mutations. J Clin Invest. 2013; 123:3664–3671. [PubMed: 23999440]

Tredan O, Galmarini CM, Patel K, Tannock IF. Drug resistance and the solid tumor microenvironment. J Natl Cancer Inst. 2007; 99:1441–1454. [PubMed: 17895480]

White E. Deconvoluting the context-dependent role for autophagy in cancer. Nat Rev Cancer. 2012; 12:401–410. [PubMed: 22534666]

Wick W, Weller M, van den Bent M, Sanson M, Weiler M, von Deimling A, Plass C, Hegi M, Platten M, Reifenberger G. MGMT testing--the challenges for biomarker-based glioma treatment. Nat Rev Neurol. 2014; 10:372–385. [PubMed: 24912512]

Young JC, Hoogenraad NJ, Hartl FU. Molecular chaperones Hsp90 and Hsp70 deliver preproteins to the mitochondrial import receptor Tom70. Cell. 2003; 112:41–50. [PubMed: 12526792]

Zhang SL, Hu X, Zhang W, Yao H, Tam KY. Development of pyruvate dehydrogenase kinase inhibitors in medicinal chemistry with particular emphasis as anticancer agents. Drug Discov Today. 2015; 20:1112–1119. [PubMed: 25842042]

SIGNIFICANCE

The ability to flexibly adapt to an unfavorable microenvironment is a distinctive feature of tumor cells, engendering treatment resistance and unfavorable disease outcome. Low oxygen pressure, or hypoxia, is a powerful driver of tumor adaptation, but "druggable" therapeutic target(s) in this response have remained elusive. Here, we show that hypoxic tumors recruit a pool of active Akt to mitochondria, culminating with Akt phosphorylation of the metabolic gatekeeper, PDK1. This phosphorylation step improves tumor fitness, preserves tumor cell proliferation in the face of severe hypoxia, and is a negative prognostic factor in glioma patients. Repurposing small molecule Akt inhibitors currently in the clinic may provide an approach to prevent hypoxic reprogramming and improve anticancer therapy.
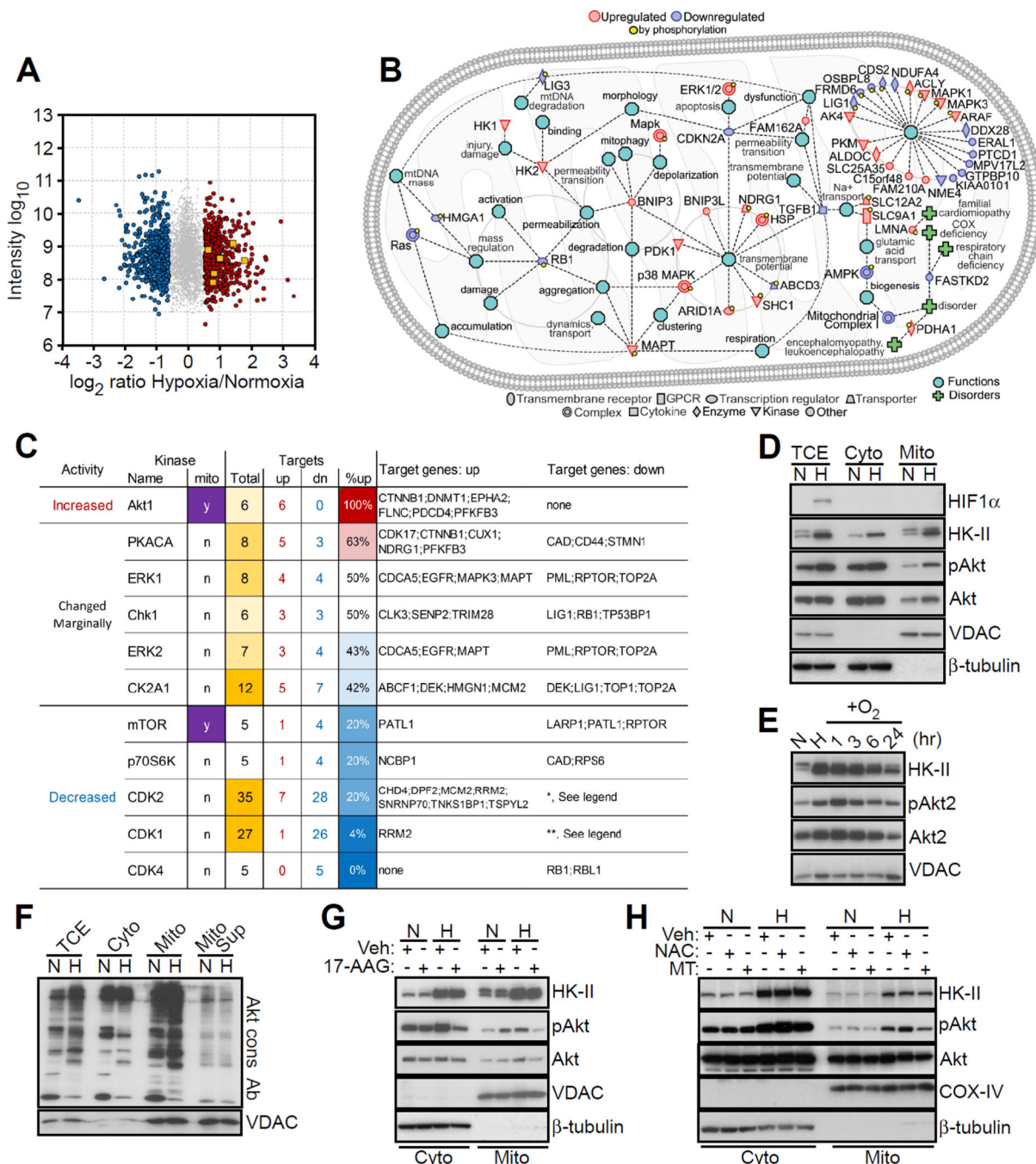
Figure 1. Mitochondrial phosphoproteome in hypoxia

(**A**) Phosphoproteome of prostate adenocarcinoma PC3 cells in hypoxia versus normoxia. Identified phosphosites met a minimum MaxQuant localization probability of 0.75 and a score difference of 5. Fold changes were calculated from the normalized Heavy/Light SILAC ratio. Six Akt target proteins showing increased phosphorylation in hypoxia are indicated. Grey, not significant; red, upregulated; blue, downregulated; yellow squares, Akt targets.

(**B**) Ingenuity pathway analysis of mitochondrial phospho- and global proteome in hypoxia.

(**C**) Kinases for which at least 5 known targets showed significant changes in phosphorylation in hypoxic versus normoxic conditions as in (A). Up, upregulation; Dn, downregulation. *, The modulated genes are: *ARID1A; HIST1H1E; HMGA1; LARP1; LIG1; LIG3; LMNB2; LRCH3; LRWD1; MARCKS; MED1; MKI67; NCL; NPM1; NUCKS1; PDS5B; PTPN2; RB1; RBL1; RBL2; SAMHD1; SETDB1; TERF2; VIM.* **, The modulated genes are: *DUT; EEF1D; HIST1H1E; HMGA1; IRS2; LIG1; LIG3; LMNA; LMNB1; MAP4; NOLC1; NPM1; NUCKS1; PDS5B; PTPN2; RB1; SAMHD1; TCOF1; TOP2A; TPX2; VIM.*

(**D**) PC3 cells in normoxia (N) or hypoxia (H) were fractionated in cytosol (Cyto) or mitochondrial (Mito) extracts and analyzed by Western blotting. pAkt, phosphorylated Akt (Ser473). TCE, total cell extracts.

(**E**) PC3 cells in hypoxia (H) were exposed to reoxygenation (O_2) for the indicated time intervals and analyzed by Western blotting. N, normoxia.

(**F**) The indicated subcellular fractions isolated from normoxic (N) or hypoxic (H) PC3 cells were analyzed with an antibody to the Akt consensus phosphorylation site RxRxxS/T (Akt cons Ab) by Western blotting. Mito Sup, supernatant of mitochondrial extracts after preclearing with Akt cons Ab.

(**G**) PC3 cells in normoxia (N) or hypoxia (H) were treated with vehicle (Veh) or Hsp90 small molecule inhibitor 17-AAG (5 μM for 6 hr), and cytosolic (Cyto) or mitochondrial (Mito) extracts were analyzed by Western blotting.

(**H**) PC3 cells in normoxia (N) or hypoxia (H) were treated with vehicle (Veh), the antioxidant N-acetyl cysteine (NAC, 1 mM) or mitochondria-specific ROS scavenger, MitoTempo (MT, 25 μM), and subcellular fractions were analyzed by Western blotting. See also Figure S1.
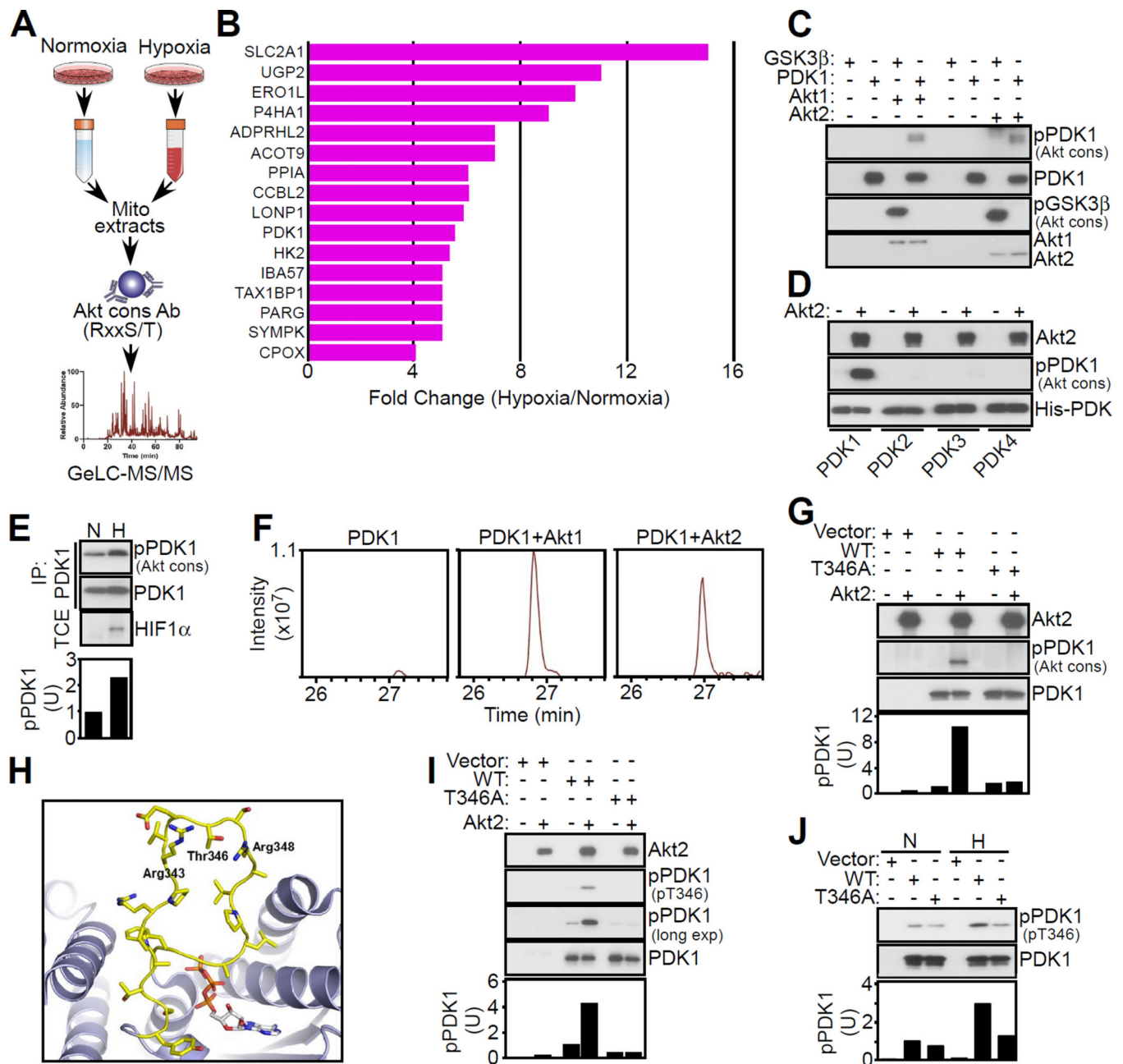
Figure 2. Mitochondrial Akt phosphorylation of PDK1

(**A**) Schematic diagram for the identification of a mitochondrial Akt phosphoproteome in hypoxic versus normoxic PC3 cells.

(**B**) Mitochondrial proteins reacting with Akt cons Ab showing differential expression in hypoxic versus normoxic PC3 cells.

(**C**) Recombinant PDK1 or GSK3β was mixed in a kinase assay with active Akt1 or Akt2, and phosphorylated bands were detected with Akt cons Ab by Western blotting.

(**D**) The indicated PDK isoforms were mixed in the presence or absence of active Akt2 in a kinase assay and phosphorylated bands were detected with Akt cons Ab, by Western blotting.

(**E**) PC3 cells in normoxia (N) or hypoxia (H) were immunoprecipitated (IP) with an antibody to PDK1 followed by Western blotting. HIF1α reactivity (bottom) was used as a marker of hypoxia. TCE, total cell extracts. Bottom, densitometric quantification of phosphorylated (p) PDK1 bands. U, arbitrary units.

(**F**) Extracted ion chromatogram of the PDK1 phosphorylated T346 chymotryptic peptide (STAPRPRVEpTSRAVPL, m/z 908.9751) resulting from incubation with or without active Akt1 or Akt2 in a kinase assay.

(**G**) PC3 cells were transfected with vector or Flag-tagged wild type (WT) PDK1 or T346A PDK1 mutant, immunoprecipitated with an antibody to Flag and immune complexes were mixed with active Akt2 in a kinase assay followed by Western blotting with Akt cons Ab. Bottom, densitometric quantification of phosphorylated (p) PDK1 bands. U, arbitrary units.

(**H**) Molecular dynamics simulation of the structure of PDK1 (ribbon) with stick representation of residues 336–356 comprising the "ATP lid". The ATP molecule is derived from the structure of PDK3-L2-ATP (PDB code 1Y8P) superimposed onto the structure of PDK1. The predicted location of Thr346 as well as Arg343 and Arg348 is shown.

(**I**) The experimental conditions are as in (**G**) except that Flag-PDK1 immune complexes mixed with active Akt2 in a kinase assay were analyzed with phospho-specific pT346 Ab by Western blotting. Exp., exposure. Bottom, densitometric quantification of phosphorylated (p) PDK1 bands. U, arbitrary units.

(**J**) Flag-PDK1 immune complexes as in (**G**) were precipitated from PC3 cells in normoxia (N) or hypoxia (H) and analyzed with pT346 Ab by Western blotting. p, phosphorylated. Bottom, densitometric quantification of pPDK1 bands. U, arbitrary units. See also Figure S2 and Table S1.
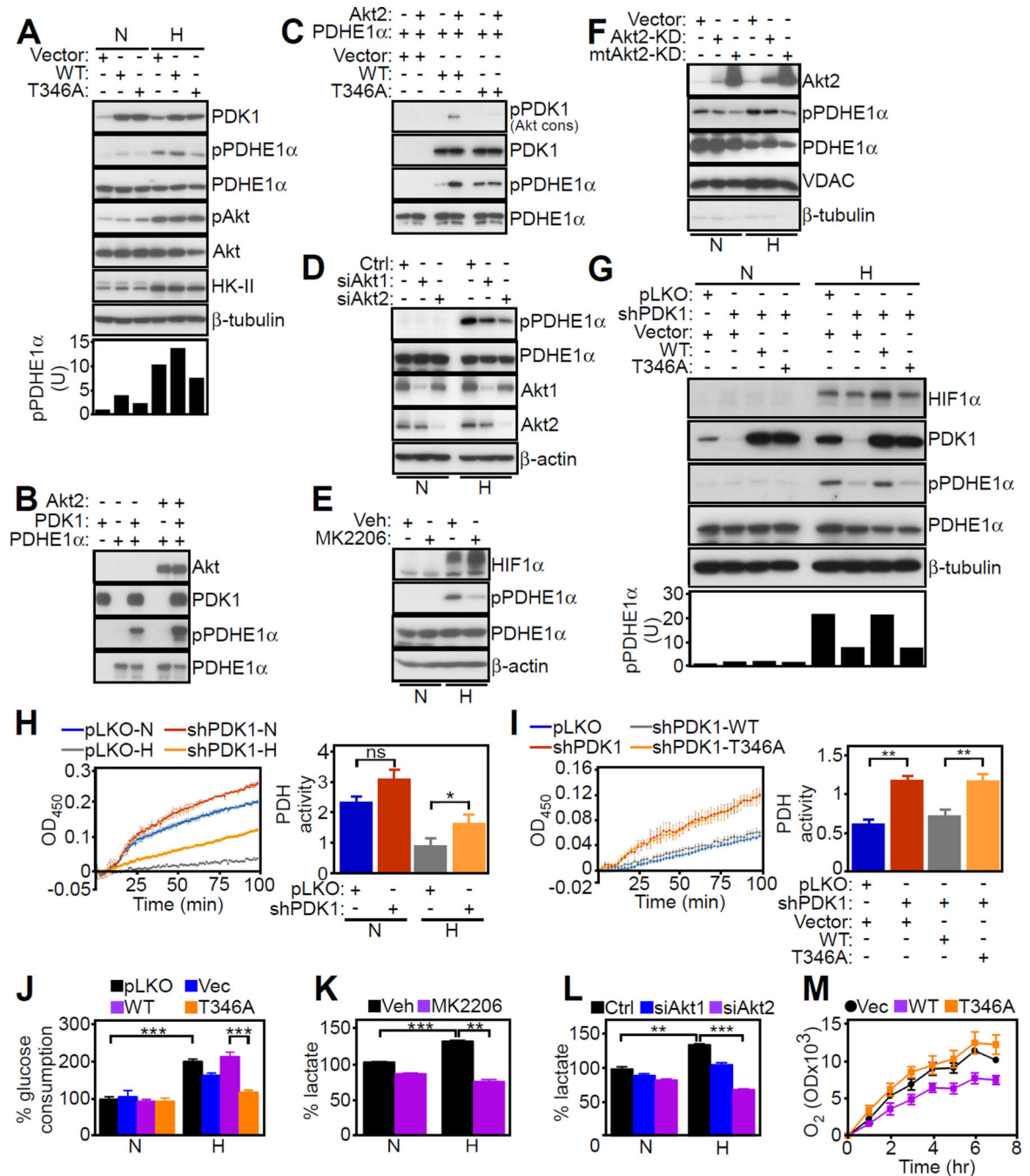
Figure 3. A mitochondrial Akt-PDK1-PDHE1 phosphorylation axis in hypoxia

(**A**) PC3 cells in normoxia (N) or hypoxia (H) were transfected with vector, WT PDK1 or T346A PDK1 mutant and analyzed by Western blotting. Bottom, densitometric quantification of phosphorylated (p) PDHE1 bands. U, arbitrary units.

(**B**) The indicated recombinant proteins were mixed in a kinase assay and analyzed by Western blotting.

(**C**) PC3 cells transfected with vector or the indicated Flag-tagged WT PDK1 or T346A PDK1 mutant were immunoprecipitated (IP) with an antibody to Flag, and immune

complexes were mixed in a kinase assay with recombinant Akt2 and PDHE1 followed by Western blotting.

(**D**) PC3 cells in normoxia (N) or hypoxia (H) were transfected with control siRNA (Ctrl) or siRNA to Akt1 or Akt2, and analyzed by Western blotting.

(**E**) PC3 cells in normoxia (N) or hypoxia (H) were treated with vehicle control (Veh) or a small molecule Akt inhibitor, MK2206 (1 μM), and analyzed by Western blotting.

(**F**) PC3 cells in normoxia (N) or hypoxia (H) were transfected with vector, Akt-kinase dead (Akt-KD) or mitochondrial-targeted Akt-KD (mtAkt-KD) mutant, and mitochondrial extracts (Mito) were analyzed by Western blotting.

(**G**) PC3 cells in normoxia (N) or hypoxia (H) were transduced with pLKO or PDK1-directed shRNA, reconstituted with vector, WT PDK1 or T346A PDK1 mutant cDNA and analyzed by Western blotting. Bottom, densitometric quantification of phosphorylated (p) PDHE1 bands. U, arbitrary units.

(**H**) PC3 cells transduced with pLKO or PDK1-directed shRNA were analyzed for PDH activity in normoxia (N) or hypoxia (H) conditions. Left, representative tracings (n=4). Right, quantification of PDH activity. ns, not significant. Mean±SEM. *, p=0.03.

(**I**) PC3 cells in hypoxia were transduced with PDK1-directed shRNA, reconstituted with vector, WT PDK1 or T346A PDK1 mutant cDNA and analyzed for PDH activity. Left, representative tracings (n=3). Right, quantification of PDH activity. Mean±SEM. **, p=0.009.

(**J**) PC3 cells transduced with pLKO or PDK1-directed shRNA were reconstituted with vector, WT PDK1 or T346A PDK1 cDNA and analyzed for glucose consumption (n=4). Mean±SEM. ***, p<0.0002.

(**K**) PC3 cells in normoxia (N) or hypoxia (H) were treated with vehicle control (Veh) or Akt inhibitor, MK2206 (1 μM), and analyzed for lactate production (n=3). Mean±SEM. **, p=0.001–0.004; ***, p=0.0005–0.0009.

(**L**) PC3 cells in normoxia (N) or hypoxia (H) were transfected with control siRNA (Ctrl) or siRNA to Akt1 or Akt2 and analyzed for lactate production (n=2). Mean±SD. **, p=0.004; ***, p=0.0005.

(**M**) PC3 cells stably silenced for PDK1 were transfected with vector (Vec), WT PDK1 or T346A PDK1 mutant, and analyzed for oxygen (O_2) consumption (n=3). Mean±SEM. For all panels, data were analyzed using the two-sided unpaired Student's t tests. See also Figure S3.
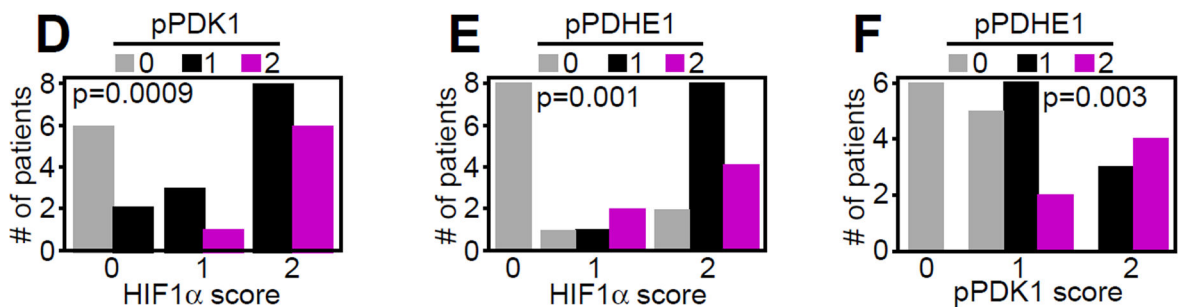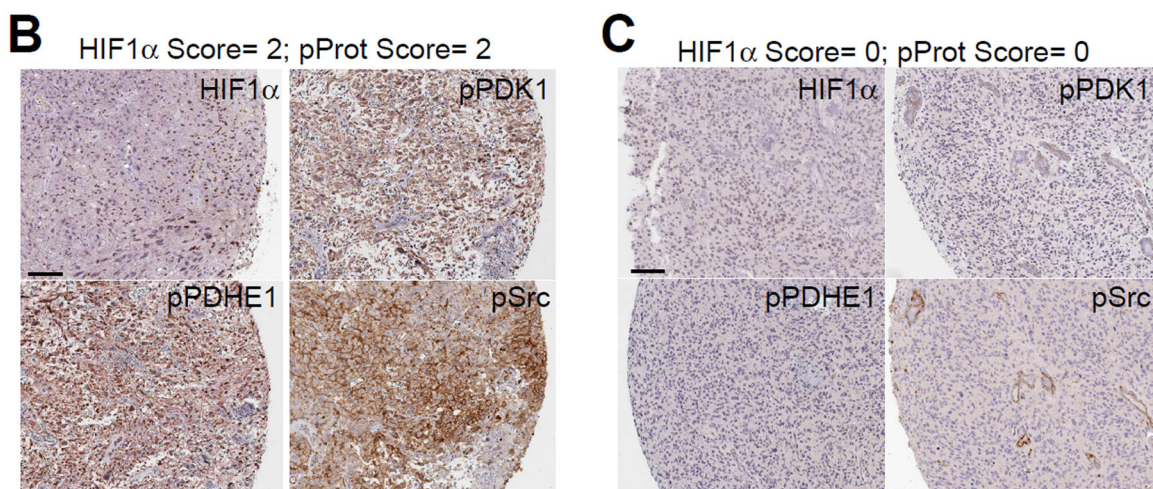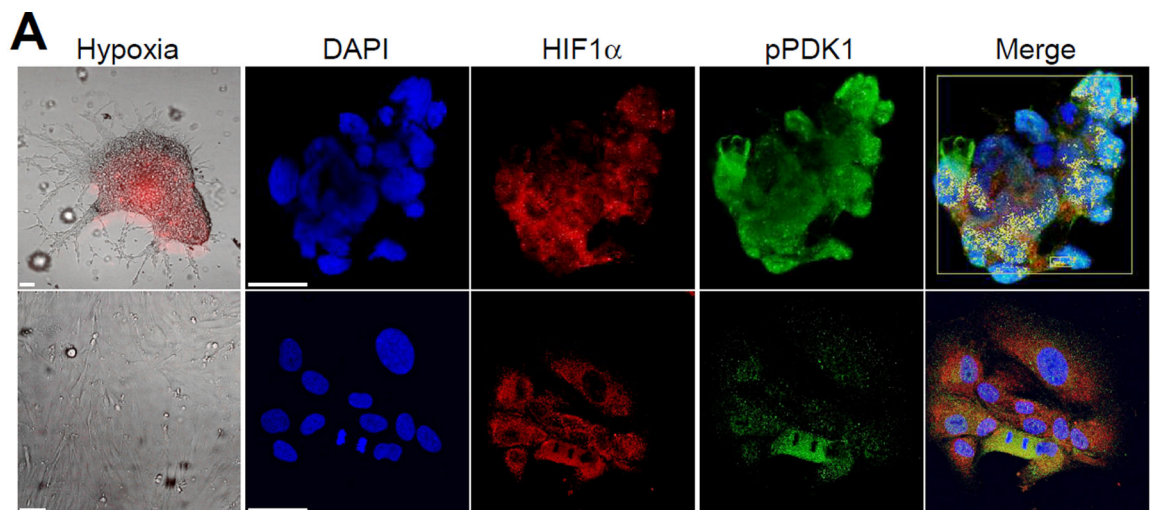
Figure 4. Mitochondrial Akt-PDK1 phosphorylation, in vivo

(**A**) GBM neurospheres (top) or differentiated GBM cultures (bottom) were stained for DNA (DAPI), HIF1α, pT346-phosphorylated PDK1, or hypoxia (hypoxia-sensitive probe). Merged images of nuclear-localized HIF1α in hypoxic neurospheres (by velocity mask) are indicated (Merge). Yellow box, Volocity analysis to identify cells with nuclear HIF1α in each single z-stack. Scale bar, 20 μm.

(**B** and **C**) Immunohistochemical staining of primary, patient-derived GBM samples with high (2) (**B**) or low (0) (**C**) score for HIF1α and phosphorylated protein (pProt) expression. Scale bar, 100 μm. p, phosphorylated.

(**D**–**F**) Quantitative immunohistochemical correlation of patient-derived GBM samples (n=24) or grade II gliomas (n=2) for HIF1α expression and pPDK1 (**D**), or pPDHE1 (**E**), or between pPDK1 and pPDHE1 (**F**). Four tissue microarray (TMA) cores/patient. The scoring is as follows: 0, no staining; 1, staining in at least one TMA core; 2, staining in 2 TMA cores. The individual p values per each analysis are indicated (Chi-Square test). See also Figure S4 and Table S2.
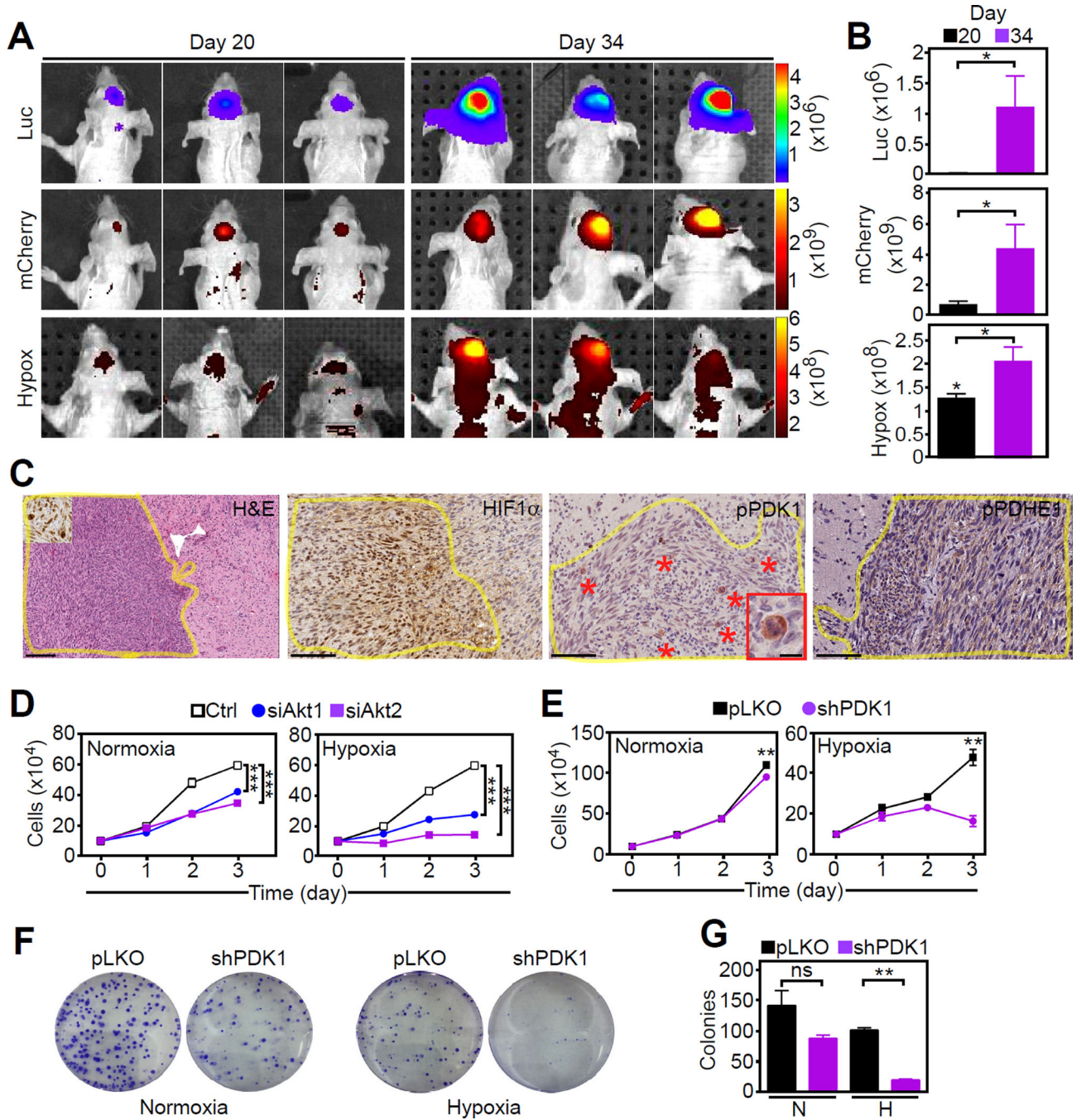
Figure 5. Requirement of mitochondrial Akt for tumor cell proliferation in hypoxia

(**A** and **B**) Bioluminescence imaging of immunocompromised mice carrying U251 intracranial GBMs (3 animals/group) expressing luciferase under the control of HIF1-responsive elements (Luc) and mCherry (cell viability) and exposed to a hypoxia-sensitive probe (Hypox). Scans were obtained at days 20 and 34 (**A**) and fluorescence signals were quantified (**B**). *, p=0.016–0.057 by Mann-Whitney test.

(**C**) Tissue samples from intracranial GBMs as in (**A**) were harvested at day 34 and analyzed for expression of HIF1α, phosphorylated (p) PDK1 (pT346 Ab) or pPDHE1, by

immunohistochemistry. Yellow lines were used to delineate the tumor mass within mice' brain. Scale bar, 100 μm. Asterisks, mitotic cells; Insets (H&E and pPDK1 panels), high-power magnification of mitotic cells. Scale bar, 25 μm.

(**D** and **E**) PC3 cells transfected with control siRNA (Ctrl) or Akt1- or Akt2-directed siRNA (**D**) or stably transduced with pLKO or PDK1-directed shRNA (**E**) were analyzed for cell proliferation in normoxia or hypoxia by direct cell counting (n=5). Mean±SEM. ***, p<0.001; **, p=0.002

(**F** and **G**) PC3 cells stably transduced with pLKO or PDK1-directed shRNA were analyzed in normoxia or hypoxia for colony formation by crystal violet staining after 10 days (**F**) and quantified (n=3) (**G**). Mean±SEM. ns, not significant. **, p=0.003. For all panels, data were analyzed using the two-sided unpaired Student's t test. See also Figure S5.
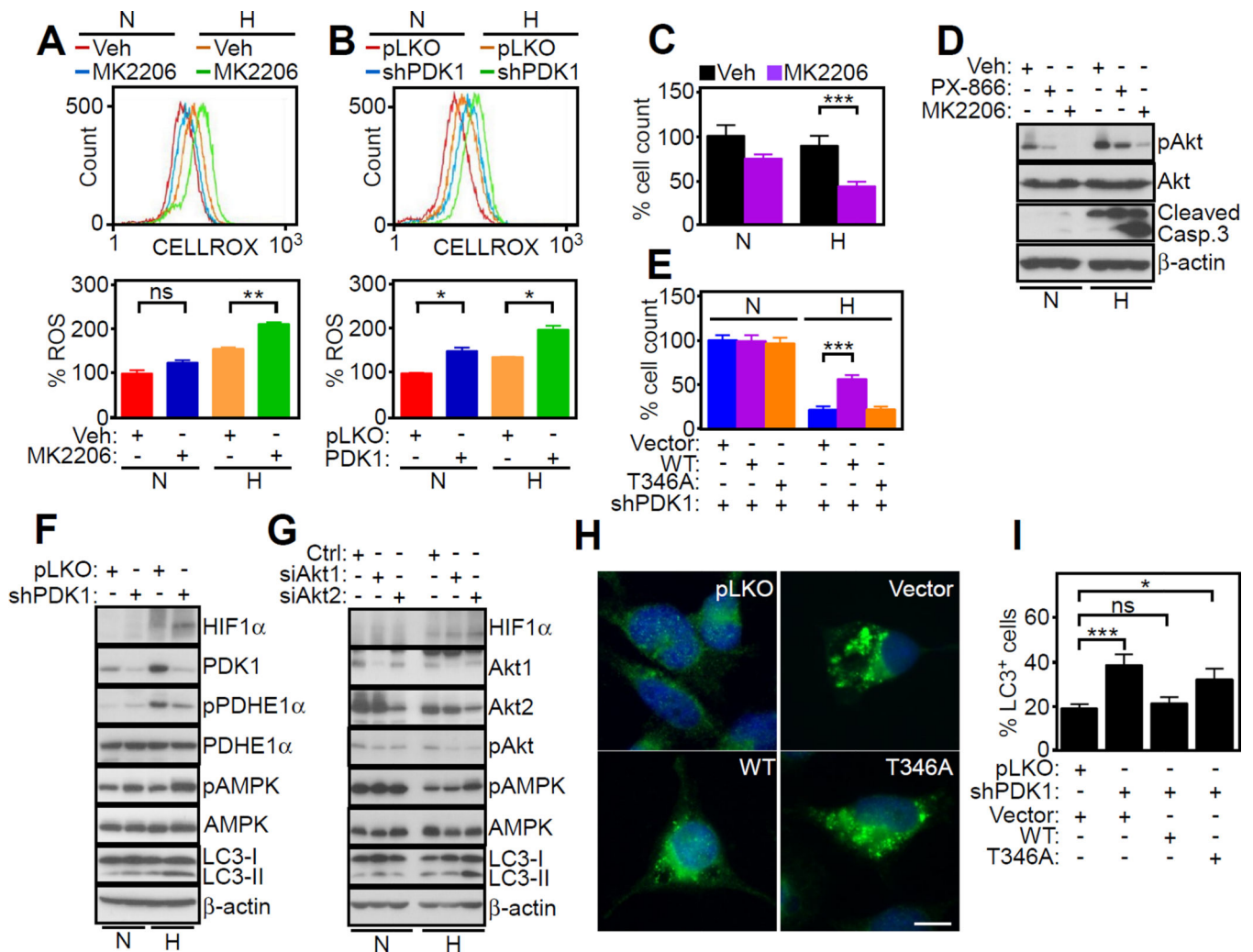
Figure 6. Mitochondrial Akt regulation of stress signaling in hypoxia

(**A** and **B**) PC3 cells in normoxia (N) or hypoxia (H) were treated with vehicle (Veh) or MK2206 (1 μM) (**A**) or transduced with pLKO or PDK1-directed shRNA (**B**) and analyzed for ROS production by CELLROX Green staining and flow cytometry. Upper panels, representative tracings. Bottom panels, quantification of ROS production under the various conditions tested (n=2). Mean±SD for both datasets. *, p=0.01–0.02; **, p=0.004; ns, not significant.

(**C**) The experimental conditions are as in (**A**) and treated cells were analyzed for cell viability by direct cell counting relative to control (n=3). Mean±SEM. ***, p<0.0001.

(**D**) PC3 cells in normoxia (N) or hypoxia (H) were incubated with vehicle (Veh) or small molecule inhibitors of Akt (MK2206, 1 μM) or PI3K (PX-866, 10 μM) and analyzed by Western blotting.

(**E**) PC3 cells stably silenced for PDK1 were reconstituted with vector, WT PDK1 or T346A PDK1 mutant and analyzed for cell viability by direct cell counting relative to control (n=3). Mean±SEM. ***, p=0.0002.

(**F** and **G**) PC3 cells in normoxia (N) or hypoxia (H) were transduced with pLKO or PDK1-directed shRNA (**F**) or control siRNA (Ctrl) or Akt1- or Akt2-directed siRNA (**G**), and analyzed by Western blotting.

(**H** and **I**) PC3 cells as in (**E**) were analyzed for LC3 reactivity by fluorescence microscopy, Scale bars, 10 μm (**H**), and cells with LC3 puncta (>3) were quantified (n=250–860 cells) (**I**). Mean±SEM.*, p=0.014; ***, p=0.0005. ns, not significant. For all panels, data were analyzed using the two-sided unpaired Student's t test. See also Figure S6.
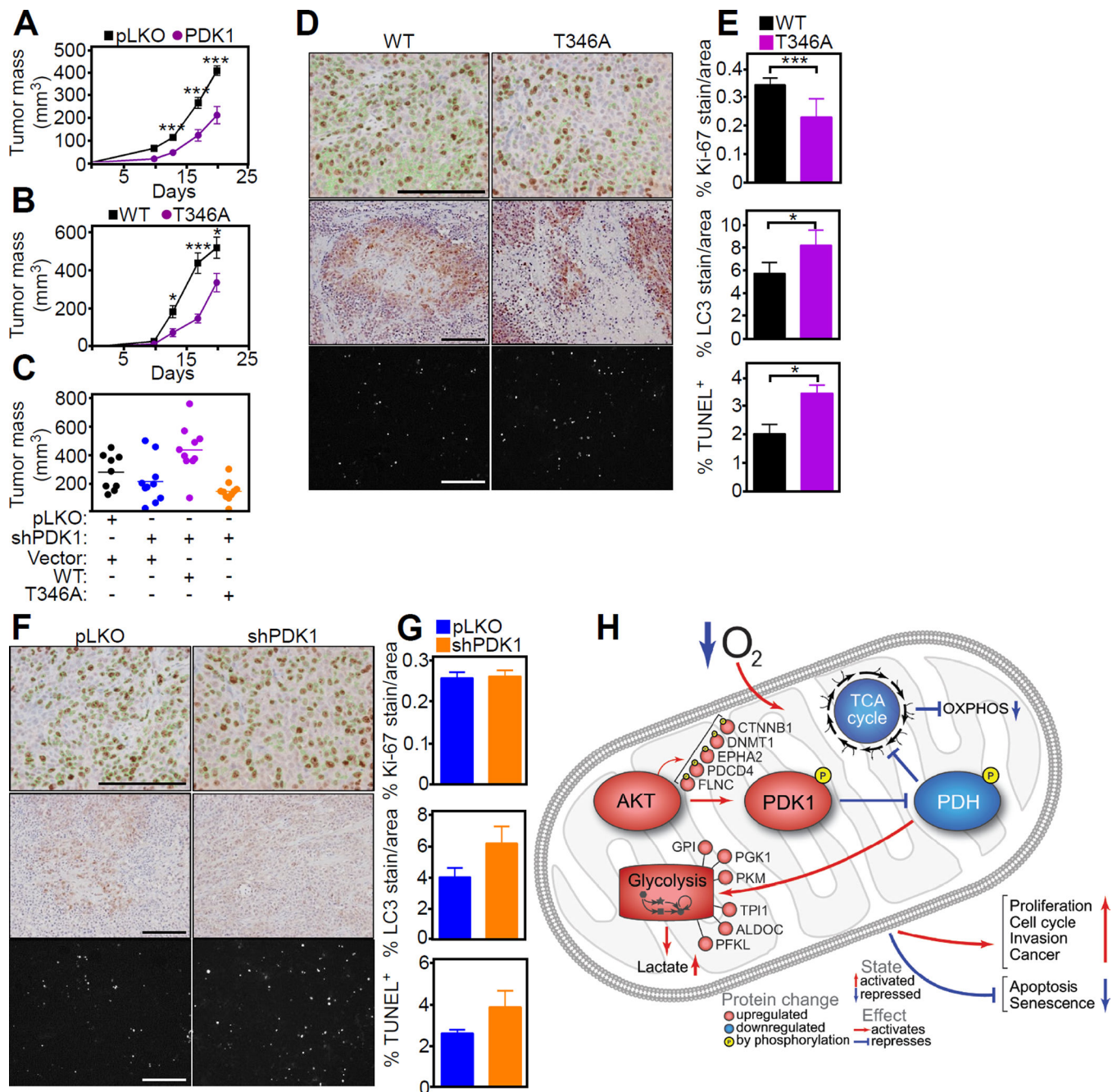
Figure 7. Mitochondrial Akt-directed hypoxic reprogramming supports tumor growth in vivo

(**A**) PC3 cells transduced with pLKO or PDK1-directed shRNA were injected s.c. in the flanks of male NSG immunocompromised mice (3 animals/group; 2 tumors/mouse) and superficial tumor growth was quantified with a caliper at the indicated time intervals for 20 days. Data were analyzed using the two-sided unpaired Student's t test. Mean±SEM. ***, p<0.0001.

(**B**) PC3 cells stably transduced with pLKO or PDK1-directed shRNA were reconstituted with WT PDK1 or T346A PDK1 mutant and injected s.c. in the flanks of immunocompromised mice (5 mice/group; 2 tumors/mouse). Tumor growth in the various

groups was quantified at the indicated time intervals for 20 days. Data were analyzed using the two-sided unpaired Student's t test. Mean±SEM. *, p=0.01–0.02; ***, p<0.0001.

(**C**) PC3 cells stably transduced with pLKO or PDK1-directed shRNA were reconstituted with vector, WT PDK1 or T346A PDK1 mutant and injected s.c. in immunocompromised mice with determination of tumor growth after 18 days. Each point corresponds to an individual tumor. (**D** and **E**) Tumors harvested from the animals in (**C**) were analyzed for histology (**D**) and cell proliferation (top, Ki-67), autophagy (middle, LC3-II) or apoptosis (bottom, TUNEL) was quantified (**E**). The statistical analysis of the various groups by ANOVA is as follows: Ki-67, p<0.0001; LC3, p=0.024; TUNEL, p=0.039. Scale bars, 100 μm.

(**F** and **G**) Superficial flank tumors of PC3 cells transduced with control pLKO or PDK1-directed shRNA were harvested after 18 day and processed for immunohistochemistry (**F**) with quantification of reactivity for Ki-67 (top), LC3 (middle) or TUNEL (bottom) (**H**). Representative images per each condition are shown. (n=3, 10 images per mouse), Mean ±SD. Scale bars, 100 μm.

(**H**) Schematic model of a mitochondrial Akt-PDK1-PDHE1 phosphorylation axis in hypoxic tumor reprogramming.
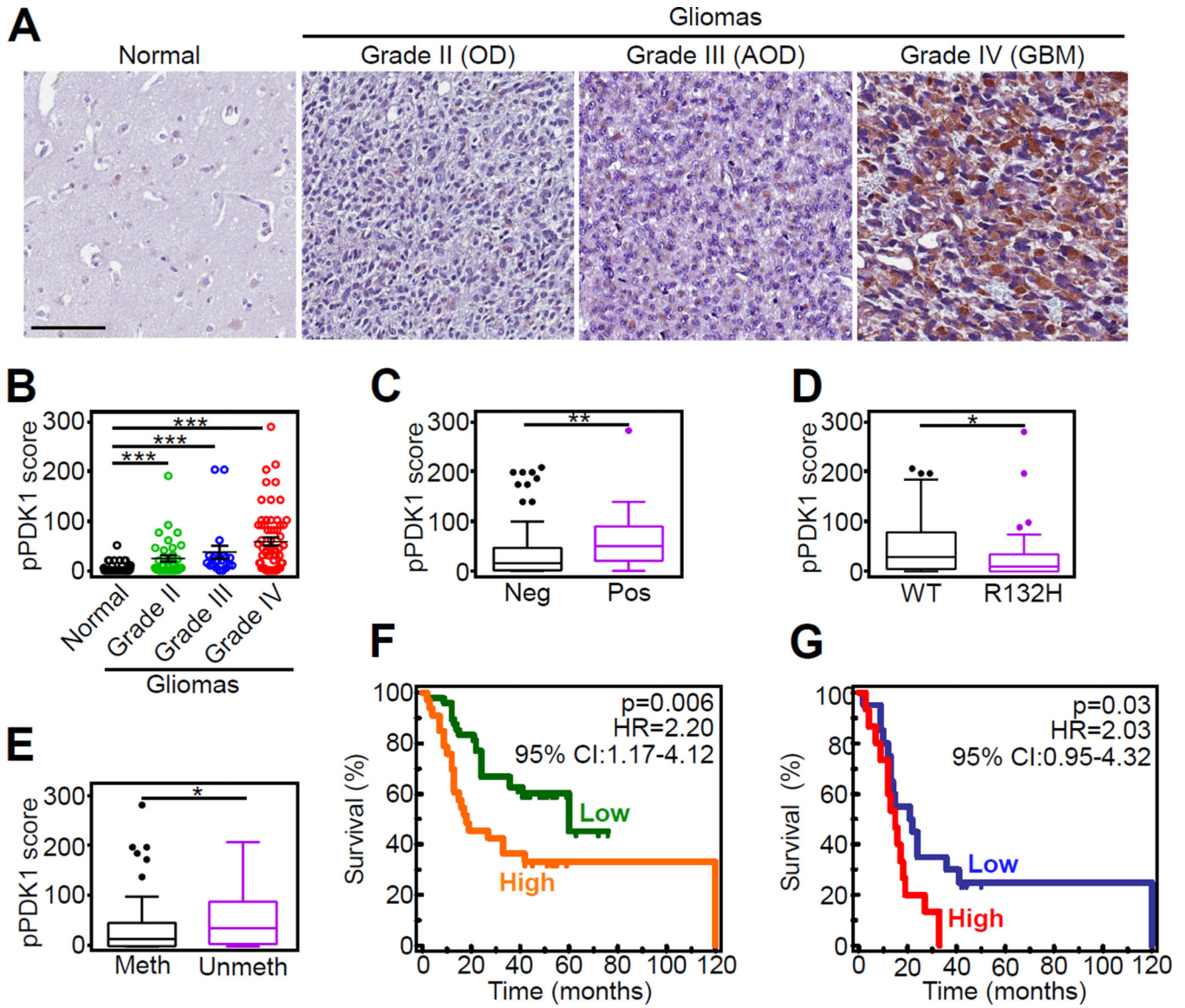
Figure 8. Mitochondrial Akt phosphorylation of PDK1 is a negative prognostic marker in human gliomas

(**A**) Representative micrographs of immunohistochemical staining of non-neoplastic human brain parenchyma (normal) or grade II-IV gliomas (WHO classification) with PDK1 pT346 Ab. OD, oligodendroglioma; AOD, anaplastic OD; GBM, glioblastoma. Scale bar, 100 μm.

(**B**) Quantification of pT346 staining in a series of human brain tumors (n=116) and 85 nonneoplastic brain parenchyma using a two-factor scoring system that considers the percentage of positive cells and the intensity of the staining (pPDK1 score). ***, p<0.0001; **, p=0.002 by Mann Whitney U-test. Each symbol represents an individual patient.

(**C–E**) Differences in pPDK1 score in human brain tumors as in (B) (n=116) according to nuclear HIF1α expression (**C**, **, p=0.008 by Mann Whitney U-test), IDH1 mutation status (**D**; *, p=0.02 by Mann Whitney U-test), or MGMT promoter methylation (**D**; *, p=0.01 by Mann Whitney U-test). Data are presented as Tukey box-and-whisker plots. The bottom and top of the box represent the first and third quartiles, and the band inside the box represents

the median (i.e. the 2nd quartile). The bottom end of the whisker represents the lowest datum within the 1.5 interquartile range (IQR) of the lower quartile, and the top end of the whisker represents the highest datum within 1.5 IQR of the upper quartile. Outlier data, if any, are represented by single points.

(**F** and **G**) Kaplan-Meier curves were generated with either the complete series of glioma patients (n=116; **F**) or with GBM cases only (n=61; **G**) sorted into "Low" or "High" groups according to pPDK1 score. Cutoffs to rank patients in these two categories were generated using ROC curves and the Youden's J statistic. Overall survival curves were compared using the Log-Rank test. HR, Hazard Ratio; CI, Confidence Interval. See also Figure S7 and Table S3.